



Do heat waves worsen air quality? A 21-year observational study in Seoul, South Korea

Kyeongjoo Park, Han-Gyul Jin ^{*}, Jong-Jin Baik ^{*}

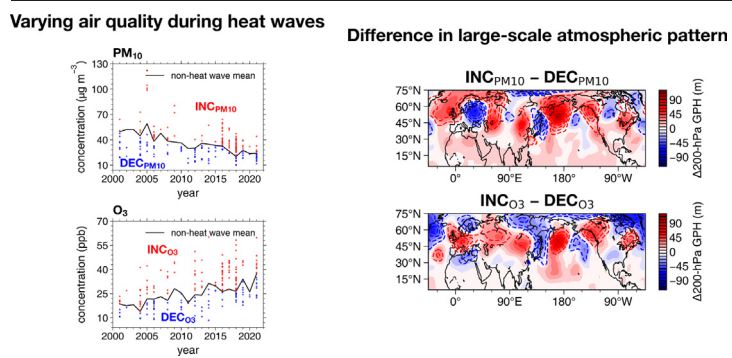
School of Earth and Environmental Sciences, Seoul National University, Seoul 08826, South Korea



HIGHLIGHTS

- Air quality changes in Seoul during heat waves are examined.
- PM₁₀ (O₃) concentration significantly decreases (increases) under heat waves.
- Impacts of heat waves on air quality vary depending on heat wave characteristics.
- Heat waves that worsen air quality show a particular large-scale atmospheric pattern.
- Heat waves with this large-scale pattern bring more stagnant conditions.

GRAPHICAL ABSTRACT



ARTICLE INFO

Editor: Jianmin Chen

Keywords:
Air quality
Heat wave
Large-scale atmospheric pattern
Ozone
Urban air pollution
Seoul

ABSTRACT

Heat waves are generally known to deteriorate air quality. However, the impacts of heat waves on air quality can substantially vary depending on the characteristics of heat waves. In this study, we examine air quality changes in Seoul during heat waves and their associations with large-scale atmospheric patterns. For this, air quality data from 25 stations and meteorological data from 23 weather stations and reanalysis datasets during July and August of 2001–2021 are used. Under heat waves, the mean daily PM₁₀, NO₂, and CO concentrations decrease by 7.9 %, 6.1 %, and 4.6 %, respectively, whereas the mean daily PM_{2.5}, O₃, and SO₂ concentrations increase by 4.1 %, 17.2 %, and 2.9 %, respectively. The atmospheric circulation under heat waves is less favorable for long-range transport of air pollutants to Seoul. The PM_{2.5}/PM₁₀ ratio increases under heat waves, indicating that the secondary formation of aerosols becomes more important under heat waves. 37 % of the heat wave days are accompanied by severe O₃ pollution exceeding the O₃ concentration standard in South Korea. There is a significant variability of air quality in Seoul within heat waves. The heat wave days with higher concentrations of PM_{2.5}, PM₁₀, O₃, NO₂, and CO than their non-heat wave means exhibit a prominent difference in large-scale atmospheric pattern from the heat wave days with lower concentrations. This difference is characterized by a zonal wave-like pattern of geopotential height, which is similar to the circumglobal teleconnection pattern known as one of the major patterns for heat waves in South Korea. This zonal wave-like pattern produces more stagnant conditions over Seoul.

1. Introduction

Heat wave, which is characterized by a prolonged period with extremely high temperature, is one of the deadliest weather-related disasters

(Goklany, 2009). The 2003 European heat wave and the 2010 Russian heat wave were estimated to cause tens of thousands of death toll (Robine et al., 2008; Barriopedro et al., 2011). In recent years, record-breaking heat waves such as the 2018 heat wave in Northeast Asia and the 2021 Western North America heat wave led to over hundreds of excess deaths (Park and Chae, 2020; BCCS, 2022). Furthermore, a number of studies projected that the heat waves will worsen due to global warming, making serious societal

* Corresponding authors.

E-mail addresses: hjin@snu.ac.kr (H.-G. Jin), jjaik@snu.ac.kr (J.-J. Baik).

problems throughout the world (e.g., Peng et al., 2011; Amengual et al., 2014; Kim et al., 2016).

Besides thermal discomfort, air pollution significantly exacerbates the risk of heat waves (Fischer et al., 2004; Stedman, 2004; Theοharatos et al., 2010; Papanastasiou et al., 2015). This is because high insolation, high temperature, and stagnant conditions under heat waves are favorable for the production and accumulation of air pollutants (Tressol et al., 2008; Kalisa et al., 2018; Wu et al., 2019). Many studies reported that air quality significantly worsens during heat waves, thereby adding negative effects on human health. Stedman (2004) investigated the air pollution-related deaths in the United Kingdom during the 2003 European heat wave and estimated that 21–38 % of total excess deaths resulted from elevated PM₁₀ and O₃ concentrations. Papanastasiou et al. (2015) showed that PM₁₀, O₃, and NO₂ concentrations clearly increase and the synergistic effect between air pollution and thermal discomfort becomes more pronounced during heat waves in Athens, Thessaloniki, and Volos in Greece. Wu et al. (2019) observed that O₃ concentration exceeded the U.S. national ambient air quality standard (70 ppb) with the maximum concentration of 110 ppb and PM_{2.5} concentration significantly increased from 5 µg m⁻³ to 25 µg m⁻³ during a heat wave event in New York City, U.S.

Meanwhile, recent studies emphasized that different types of large-scale atmospheric patterns related to heat waves can lead to significantly different air quality and showed that there are particular large-scale atmospheric patterns that substantially aggravate air quality during heat waves. Yang et al. (2022) analyzed the daily maximum 8-hour average O₃ concentration in the Beijing-Tianjin-Hebei region in China. They showed that heat waves that significantly increase O₃ concentration are usually associated with stable saddle-like circulation anomalies and atmospheric blocking, whereas heat waves with wave-train circulation anomalies do not significantly increase O₃ concentration. Ruiz-Páez et al. (2023) identified two types of heat waves in Spain. They showed that PM₁₀ concentration is higher under heat waves accompanied by warm and dust advection from the Saharan desert (33.6 µg m⁻³) than under those with stagnant anticyclonic conditions (22.2 µg m⁻³), resulting in more harmful health effects. These studies reveal that changes in air quality during heat waves can significantly vary depending on the meteorological origins and characteristics of heat waves.

Heat waves occurring in South Korea (Fig. 1a) are associated with various factors such as regional atmospheric systems (e.g., the western North Pacific subtropical high, the Tibetan high), teleconnection patterns

(e.g., the Pacific-Japan pattern, the circumglobal teleconnection pattern), and blocking patterns (e.g., the Kamchatka blocking) (Lee and Lee, 2016; Yeh et al., 2018; Yeo et al., 2019; Lee et al., 2020a; Yoon et al., 2020; Choi et al., 2021; Noh et al., 2021; Cha et al., 2022). Consequently, air quality during heat waves in South Korea may considerably vary depending on which types of large-scale atmospheric patterns are associated with heat waves. Especially, Seoul, which is the largest city in South Korea, is faced with large risks of thermal discomfort originating from urban heat islands and heat waves and air pollution caused by local emission and long-range transport (Jeong et al., 2017; Hong et al., 2019; Bae et al., 2020; Park et al., 2021). However, there are no studies that examine how air quality changes during heat waves in Seoul are associated with large-scale atmospheric patterns. This study aims to investigate how air quality in Seoul changes during heat waves and find large-scale atmospheric patterns significantly affecting air quality during heat waves. Section 2 describes the data and method used in this study. In Section 3, results and discussion are presented. The summary and conclusions are given in Section 4.

2. Data and method

2.1. Data

This study analyzes PM_{2.5}, PM₁₀, O₃, NO₂, CO, and SO₂ concentrations obtained from 25 air quality monitoring stations (AQMSs) in Seoul during July and August of 2001–2021 (Fig. 1b). The 25 AQMSs are operated by the Seoul Health and Environment Institute (SHEI), and hourly-averaged pollutant concentrations are screened and provided by the Korea Environment Corporation (<https://airkorea.or.kr>). These data are available since 2001 for PM₁₀, O₃, NO₂, CO, and SO₂ and since 2015 for PM_{2.5}. For PM_{2.5} data before 2015, the data provided directly by SHEI (<https://data.seoul.go.kr>) are used after excluding the data classified as abnormal by the observation instrument and the data with the PM_{2.5} concentration value exceeding the PM₁₀ concentration value. To analyze meteorological variables associated with air quality, 23 weather stations in Seoul are selected (Fig. 1b). The selected weather stations consist of one automated synoptic observing system (ASOS) and 22 automatic weather stations (AWSs) operated by the Korea Meteorological Administration. Their elevations are < 150 m. Daily maximum 2-m temperature, daily mean and hourly 2-m temperature, and daily mean and hourly 10-m wind speed are obtained from those weather stations. Daily mean and hourly relative humidity

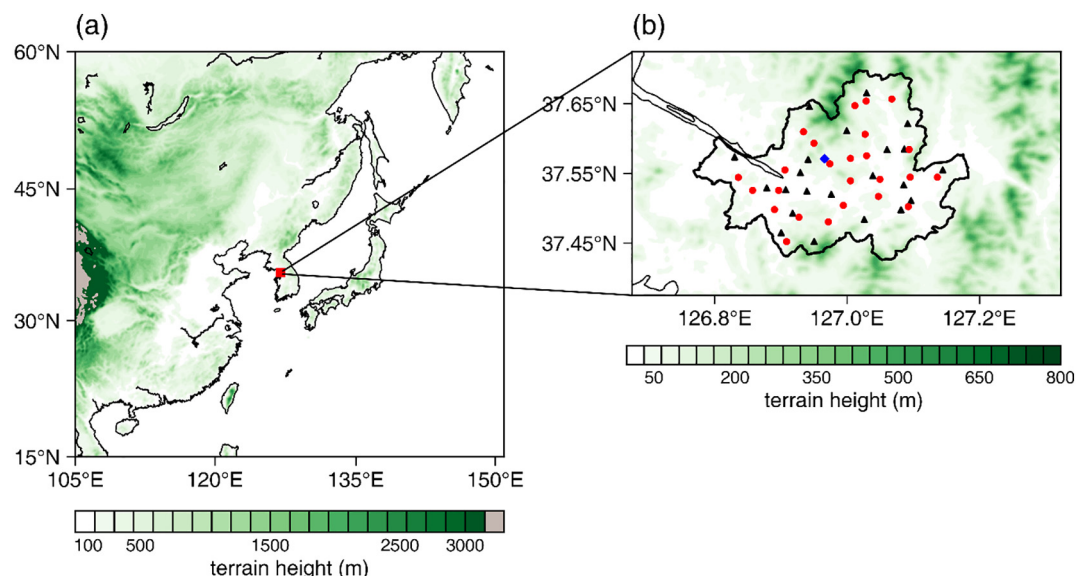


Fig. 1. (a) Geographical location of South Korea. The study area is denoted by the red rectangle. (b) Locations of the air quality monitoring stations (AQMSs, red circles), one automated synoptic observing system (ASOS, blue diamond), and 22 automatic weather stations (AWSs, black triangles). The border of Seoul is indicated by the thick solid line. The color shades in (a) and (b) indicate terrain height.

(RH_{avg}), daily mean cloud cover (CC_{avg}), and daily total insolation are additionally obtained from the ASOS.

To investigate the atmospheric patterns associated with air quality, the geopotential heights at the 200- and 500-hPa levels, zonal and meridional wind speeds at the 500- and 850-hPa levels, and boundary layer height (BLH) are acquired from the fifth-generation European Centre for Medium-range Weather Forecasts (ECMWF) reanalysis (ERA5) data (Hersbach et al., 2020). In the ERA5, BLH is defined as the minimum height where the bulk Richardson number reaches 0.25 (Kim, 2022; Slättberg et al., 2022). BLH obtained from the ERA5 was validated using worldwide radiosonde data and showed good accuracy (Guo et al., 2021). Allabakash and Lim (2020) also showed that BLH from the ERA5 agrees well with that derived from radiosonde measurements in South Korea. The horizontal resolution and temporal resolution of the ERA5 data are $0.25^\circ \times 0.25^\circ$ and 1 h, respectively. To analyze the long-range transport of air pollutants, $PM_{2.5}$ column density, CO column density, and SO_2 column density are obtained from the Modern-Era Retrospective analysis for Research and Applications version 2 (MERRA-2) data (Gelaro et al., 2017). The $PM_{2.5}$ column density is calculated from dust, sea salt, organic carbon, black carbon, and sulfate column densities in the MERRA-2 data following Jin et al. (2022) where the $PM_{2.5}$ concentration [$PM_{2.5}$] is calculated as

$$[PM_{2.5}] = [DUST_{2.5}] + [SS_{2.5}] + [BC] + 1.6 \times [OC] + 1.375 \times [SO_4]. \quad (1)$$

Here, $[DUST_{2.5}]$ and $[SS_{2.5}]$ denote the concentrations of dust and sea-salt with diameter $< 2.5 \mu m$, respectively, and $[BC]$, $[OC]$, and $[SO_4]$ denote the concentrations of black carbon, organic carbon, and sulfate, respectively. The horizontal resolution of the MERRA-2 data is $0.5^\circ \times 0.625^\circ$, and the temporal resolution is 1 h for $PM_{2.5}$, CO, and SO_2 column densities. The O_3 mixing ratio at the 850-hPa level is obtained from the Copernicus Atmosphere Monitoring Service reanalysis (CAMSRA) to analyze the transport of tropospheric O_3 (Inness et al., 2019). Park et al. (2020) pointed out that the CAMSRA is more suitable for tropospheric O_3 analysis in East Asia than the ERA5 and MERRA-2. The CAMSRA data are available since 2003 and have a temporal resolution of 3 h and a horizontal resolution of $0.75^\circ \times 0.75^\circ$.

2.2. Method

We analyze daily mean concentrations of six air pollutants ($PM_{2.5}$, PM_{10} , O_3 , NO_2 , CO, and SO_2) averaged over the 25 AQMSs. Daily mean 2-m temperature and 10-m wind speed are averaged over the 23 weather stations, denoted by T_{avg} and $WS10_{avg}$, respectively. Before taking the average over the stations, the meteorological data on the days when the daily precipitation amount is larger than 0.1 mm are excluded. The air pollutant concentration data on the days when the daily precipitation amount at the nearest weather station is larger than 0.1 mm are excluded. Daily mean 850-hPa wind speed over the Korean Peninsula ($35\text{--}40^\circ N$, $125\text{--}130^\circ E$) and BLH at the grid point in Seoul ($37.5^\circ N$, $127.0^\circ E$) are also calculated and denoted by $WS850_{avg}$ and BLH_{avg} , respectively, in order to examine the impacts of synoptic wind speed in the lower troposphere and boundary layer height.

This study defines a heat wave (HW) as a period of two or more consecutive days on which the daily maximum 2-m temperature averaged over all the meteorological stations (T_{max}) exceeds $33^\circ C$. Following many studies on heat waves in South Korea (e.g., Lee and Lee, 2016; Yoon et al., 2020;

Table 2

Mean daily $PM_{2.5}$, PM_{10} , O_3 , NO_2 , CO, and SO_2 concentrations under HW and nonHW and their respective differences (HW minus nonHW). For the differences, the statistical significances are given. The numbers in the brackets indicate relative changes (%).

	$PM_{2.5}$ ($\mu g m^{-3}$)	PM_{10} ($\mu g m^{-3}$)	O_3 (ppb)	NO_2 (ppb)	CO (ppb)	SO_2 (ppb)
HW	21.0	34.4	29.0	22.2	396.5	3.9
nonHW	20.1	37.4	24.7	23.6	415.7	3.8
HW –	0.8	-2.9*	4.2*	-1.4*	-19.2*	0.1
nonHW	[4.1 %]	[-7.9 %]	[17.2 %]	[-6.1 %]	[-4.6 %]	[2.9 %]

* Statistically significant ($p < 0.05$).

Choi et al., 2021), we adopt the $33^\circ C$ and the two days as the thresholds. In July and August of 2001–2021, total 210 days are identified as HW days and the remaining 1092 days are categorized as non-heat waves (nonHW) days. As noted above, the data of the days with precipitation (>0.1 mm) are excluded for both HW and nonHW days. Excluding the five days when the pollutant concentration data at all AQMSs are removed because of precipitation, 205 HW days remain. The HW days are further classified into two groups, INC_x and DEC_x, for each pollutant x ($PM_{2.5}$, PM_{10} , O_3 , NO_2 , CO, or SO_2). INC_x (DEC_x) is defined as the HW days with increased (decreased) daily concentration of pollutant x than its nonHW mean for the corresponding year. This classification is used to examine the characteristics of heat waves that improve or worsen air quality.

Table 1 presents meteorological conditions averaged for HW and nonHW. HW shows significantly higher T_{avg} , lower RH_{avg} , lower CC_{avg} , and lower $WS850_{avg}$ than nonHW. The 10-m wind speed during the daytime (13–17 local standard time, hereafter LST) does not exhibit a significant difference between HW and nonHW, but the 10-m wind speed during the nighttime (01–05 LST) is significantly lower under HW than under nonHW. BLH during the daytime is significantly higher under HW than under nonHW, but BLH during the nighttime is significantly lower. The lower nighttime BLH under HW may be related to the lower nighttime wind speed under HW, as low wind speed inhibits vertical mixing (Martilli, 2002).

3. Results and discussion

3.1. Air quality under HW and nonHW

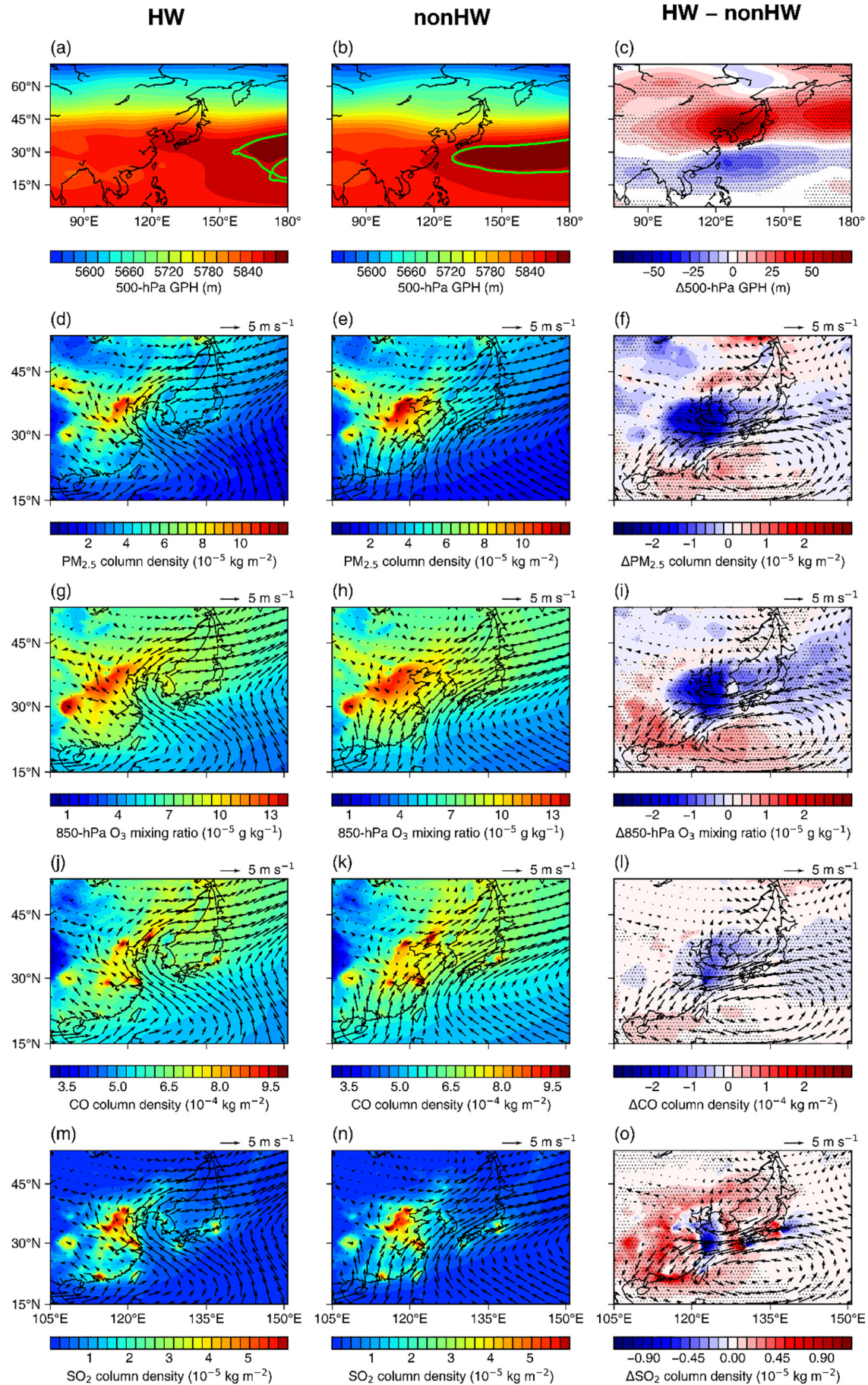
Table 2 shows the mean daily $PM_{2.5}$, PM_{10} , O_3 , NO_2 , CO, and SO_2 concentrations under HW and nonHW. Compared to nonHW, the daily PM_{10} , NO_2 , and CO concentrations under HW statistically significantly ($p < 0.05$) decrease by 7.9 %, 6.1 %, and 4.6 %, respectively. Contrary to PM_{10} , the $PM_{2.5}$ concentration increases by 4.1 %, though the increase is statistically insignificant. The daily O_3 concentration significantly increases by 17.2 %. The daily SO_2 concentration increases (2.9 %) under HW, but the increase is statistically insignificant. Several studies pointed out that high temperature and stagnant conditions during heat waves can promote the accumulation and secondary formation of aerosols (e.g., Churkina et al., 2017; Kalisa et al., 2018; Wu et al., 2019). In Seoul, the $PM_{2.5}$ concentration increases under HW, but the PM_{10} concentration decreases. This means that the decrease in PM_{10} concentration under HW is driven by the decrease in the concentration of relatively coarse particulate matters. The

Table 1

Mean T_{avg} , RH_{avg} , CC_{avg} , $WS850_{avg}$, daytime (13–17 LST)/nighttime (01–05 LST) 10-m wind speed, and daytime/nighttime BLH under HW and nonHW and their respective differences (HW minus nonHW). For the differences, the statistical significances are given. The numbers in the brackets indicate relative changes (%).

	T_{avg} ($^\circ C$)	RH_{avg} (%)	CC_{avg}	$WS850_{avg}$ ($m s^{-1}$)	10-m wind speed (daytime/nighttime) ($m s^{-1}$)	BLH (daytime/nighttime) (m)
HW	29.6	63.4	3.7	5.26	2.10/1.05	1085.2/115.7
nonHW	25.9	68.1	5.9	7.38	2.10/1.28	838.9/237.3
HW – nonHW	3.7* [14.2 %]	-4.7* [-6.9 %]	-2.2* [-36.8 %]	-2.12* [-28.7 %]	0.00/-0.23* [0.0 %/-17.8 %]	246.3*/-121.6* [29.4 %/-51.2 %]

* Statistically significant ($p < 0.05$).



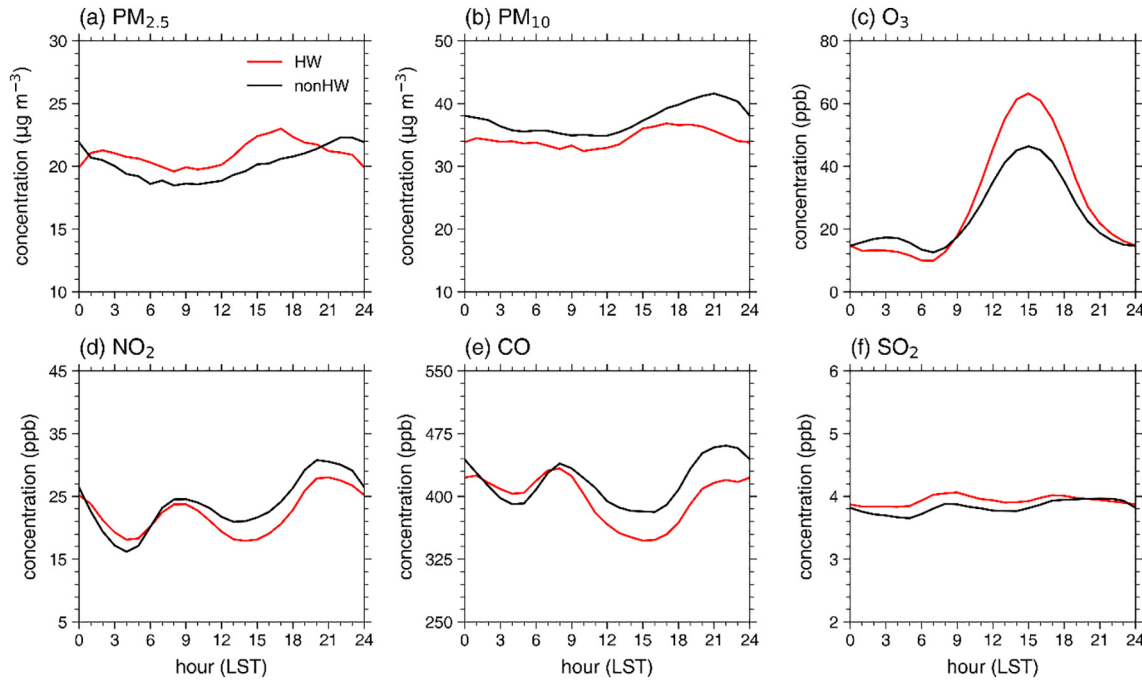


Fig. 3. Diurnal variations of (a) PM_{2.5}, (b) PM₁₀, (c) O₃, (d) NO₂, (e) CO, and (f) SO₂ concentrations under HW (red) and nonHW (black).

PM_{2.5–10} concentration, which is the PM₁₀ concentration minus the PM_{2.5} concentration, significantly decreases by 22.2 % under HW. As a result, the PM_{2.5}/PM₁₀ ratio under HW (0.62) is significantly higher than that under nonHW (0.56). Given that the secondary formation of aerosols is highly related to PM_{2.5} rather than PM_{2.5–10} (Ghim et al., 2015; Zhang and Cao, 2015; Lee et al., 2018; Park et al., 2022), the increase in PM_{2.5}/PM₁₀ ratio under HW suggests that the secondary formation of aerosols becomes more relatively important under HW.

The impacts of atmospheric circulation change under HW are examined. Fig. 2 shows composite 500-hPa synoptic fields and composite fields of PM_{2.5} column density, O₃ mixing ratio at the 850-hPa level, CO column density, and SO₂ column density with 850-hPa horizontal wind vector under HW and nonHW, as well as their respective differences. At the 500-hPa level, an anticyclonic circulation is dominant over the Korean Peninsula under HW due to an anomalous high (Fig. 2a and c). The dominant anticyclonic circulation is also seen at the 850-hPa level (Fig. 2d, g, j, and m). Under nonHW, the western boundary of the western North Pacific subtropical high (WNPSH) is expanded to the south of the Korean Peninsula (Fig. 2b). Along the boundary of the WNPSH, southwesterly winds prevail over South Korea (Fig. 2e, h, k, and n). This circulation difference between HW and nonHW affects the long-range transport of air pollutants. Note that the long-range transport of aerosols is known to be an important factor that modulates air quality in East Asia (e.g., Chen et al., 2017; Jeong et al., 2017; Li et al., 2019; Bae et al., 2020). Under nonHW, an area of high PM_{2.5} column density is expanded from Eastern China to the Korean Peninsula along the prevailing southwesterly winds (Fig. 2e). Under HW, the area of high PM_{2.5} column density is expanded deep into Northeastern China along the anticyclonic circulation, and the Yellow Sea and the Korean Peninsula are relatively less affected by this expansion (Fig. 2d). As a result, an area of strong negative PM_{2.5} column density difference covers the Yellow Sea and the Korean Peninsula, along the southern part of the anticyclonic circulation difference (Fig. 2f). The PM_{2.5} column density over the Korean Peninsula under HW is 16.3 % smaller compared to nonHW, and that

over the Yellow Sea region (35–40°N and 120–125°E) is 23.2 % smaller under HW. These suggest that the atmospheric circulation change under HW leads to the reduction of long-range transport of aerosols to the Korean Peninsula. Lee et al. (2021) also pointed out that the long-range transport of aerosols from southeastern China by the southwesterly winds affects Seoul in summer.

The 850-hPa O₃ mixing ratio and the CO column density also exhibit similar decreasing patterns around the Korean Peninsula under HW, associated with the atmospheric circulation change (Fig. 2i and l). This indicates that the atmospheric circulation under HW is less favorable for long-range transport of gaseous pollutants to the Korean Peninsula as well as for that of aerosols. Note that the 850-hPa O₃ mixing ratio in South Korea does not decrease despite the reduction of long-range transport, possibly because of the increased photochemical production of O₃ in South Korea under HW. Meanwhile, the SO₂ column density increases under HW throughout South Korea (Fig. 2o). Power plants are major sources of SO₂ in South Korea (<https://me.go.kr>). During heat waves, electric power generation can be increased to meet the increased demand of cooling energy, leading to increased emission of SO₂ (Abel et al., 2017).

Fig. 3 shows diurnal variations of PM_{2.5}, PM₁₀, O₃, NO₂, CO, and SO₂ concentrations under HW and nonHW. The PM_{2.5} concentration under HW is higher than that under nonHW at most hours (Fig. 3a). It peaks at 17 LST, 5 h earlier than the peak time under nonHW, possibly associated with the enhancement of daytime secondary formation of aerosols (Papanastasiou et al., 2010; Kalisa et al., 2018; Wu et al., 2019). The PM₁₀ concentration is lower under HW than under nonHW throughout the day, possibly contributed by the reduced long-range transport of aerosols (Fig. 2f). The PM₁₀ concentration exhibits a diurnal variation with a single prominent peak similar to that of PM_{2.5} concentration under both HW and nonHW because PM_{2.5} accounts for a considerable portion of PM₁₀ concentration (HW: 0.62, nonHW: 0.56). The other portion of PM₁₀ concentration (PM_{2.5–10}) exhibits two prominent peaks in the morning and evening (not shown), similar to the NO₂ concentration. The PM_{2.5} and PM₁₀ diurnal

Fig. 2. (a, b, c) Composite fields of 500-hPa geopotential height (GPH) under HW and nonHW and their differences (HW minus nonHW). The green contour line (5880 m) indicates the boundary of the western North Pacific subtropical high (WNPSH). (d, e, f) Composite fields of PM_{2.5} column density with 850-hPa horizontal wind vector under HW and nonHW and their respective differences (HW minus nonHW). (g, h, i) The same as (d, e, f) except for 850-hPa O₃ mixing ratio. (j, k, l) The same as (d, e, f) except for CO column density. (m, n, o) The same as (d, e, f) except for SO₂ column density. The dotted area in (c), (f), (i), (l), and (o) indicates statistical significance at $p < 0.05$.

variations with a single prominent peak are characteristic features observed in summertime Seoul that are seldom observed in other cities in South Korea (Kim et al., 2020), which deserves future investigation.

The change in O₃ concentration under HW is contrasting between the daytime and nighttime (Fig. 3c). During the daytime, the O₃ concentration is considerably higher under HW than under nonHW, showing a relative change of 35.0 %. The daily maximum of 8-hour average O₃ concentration (MDA8) increases from 41.0 ppb (nonHW) to 54.2 ppb (HW). 37 % of the total HW days (78 days) exceed the O₃ concentration standard in South Korea (60 ppb). Thus, a number of HW days have high thermal risks and severe ozone pollution at the same time. The prominent increase in O₃ concentration during the daytime can be associated with relatively high insolation and high temperature under HW, which promote the chemical production of O₃ (Pu et al., 2017; Wu et al., 2017; Pyrgou et al., 2018; Zhao et al., 2019).

The elevated daytime O₃ concentration under HW may be associated with the 5-hour earlier appearance of the peak time of PM_{2.5} concentration at 17 LST, which is two hours after the peak time of O₃ concentration (Fig. 3a). A high O₃ concentration increases the atmospheric oxidation capacity (Wang et al., 2015; Chen et al., 2020), and the increased atmospheric oxidation capacity promotes the formation of secondary aerosols such as nitrate, sulfate, and organic matters, which are dominant PM_{2.5} chemical compositions in Seoul (Lee et al., 2020b; Kim et al., 2021; Wang et al., 2023). This can be one possible reason for the shift of the peak time of PM_{2.5} concentration under HW.

During the nighttime, the O₃ concentration is lower under HW than under nonHW. Furthermore, the nighttime secondary maximum that occurs under nonHW is diminished under HW. During the nighttime, the vertical mixing between the residual layer and the layer below elevates the near-surface O₃ concentration (Tong et al., 2011), which is the reason for the appearance of nighttime secondary maximum under nonHW. The decreased 10-m wind speed and BLH during the nighttime under HW (Table 1) can decrease the vertical mixing and consequently decrease the nighttime O₃ concentration. During the whole study period, the nighttime O₃ concentration has statistically significant positive correlations with the nighttime 10-m wind speed and BLH with the Pearson's correlation coefficients (*R*) being 0.34 and 0.34, respectively.

The NO₂ and CO concentrations show clear bimodal diurnal variations with peaks in the morning and evening (Fig. 3d and e). Both NO₂ and CO concentrations exhibit declines after the morning peaks, and these declines are steeper under HW than under nonHW. After the declines, the NO₂ and CO concentrations under HW stay lower than those under nonHW. These can be due to the relatively high BLH (Table 1) and active chemical reactions and consumption of NO₂ and CO associated with the high O₃ concentration under HW (Kim et al., 2018; Kim and Kim, 2020; Lee and Park, 2022), contributing to the lower NO₂ and CO concentrations under HW (Table 2). Kim and Kim (2020) also pointed out that CO concentration tends to become low under high O₃ concentration due to the reaction with the hydroxyl radical (OH). SO₂ shows relatively weak diurnal variation under both HW and nonHW (Fig. 3f). A slight increase in SO₂ under HW is seen in most hours.

Fig. 4 shows individual values of daily concentrations of the six air pollutants under HW for each year with the interannual variations of their annual-mean concentrations under HW and nonHW. The long-term trends of the air pollutants under nonHW are consistent with the results of previous studies (Kim and Lee, 2018; Lee et al., 2018; Seo et al., 2018). The PM_{2.5}, PM₁₀, NO₂, and CO concentrations show significantly decreasing trends for 2001–2021, whereas the O₃ concentration shows a significantly increasing trend. It is noteworthy that the decreasing trend of PM₁₀ ($-1.54 \mu\text{g m}^{-3} \text{ year}^{-1}$) is much steeper than that of PM_{2.5} ($-0.47 \mu\text{g m}^{-3} \text{ year}^{-1}$). Lee et al. (2018) showed that the increasing trend of surface air temperature promotes the secondary formation of fine particles and leads to more gradual decreasing trend of PM_{2.5} than that of coarser particles. The SO₂ concentration does not exhibit a significant trend and is very low compared to the SO₂ concentration standard in South Korea (20 ppb).

The HW-mean pollutant concentrations are higher than the nonHW means in some years (e.g., 2016 and 2017, for all pollutants except SO₂) and lower than the nonHW means in other years (e.g., 2014, for all pollutants except SO₂). Daily pollutant concentrations under HW are widely distributed and can be either higher or lower than their nonHW means. Out of the total 205 HW days analyzed, 113 (91), 95 (110), 125 (80), 111 (94), 92 (113), and 102 (103) HW days show higher (lower) PM_{2.5}, PM₁₀, O₃, NO₂, CO, and SO₂ concentrations than their nonHW means for the corresponding

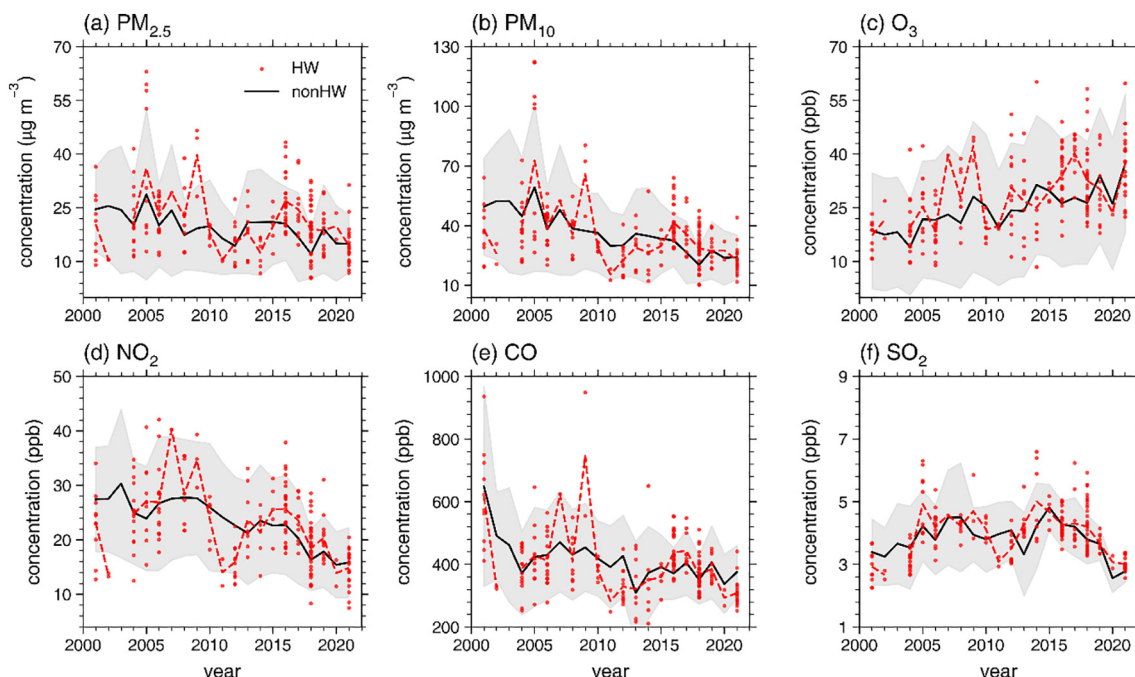


Fig. 4. All values of daily concentrations of (a) PM_{2.5}, (b) PM₁₀, (c) O₃, (d) NO₂, (e) CO, and (f) SO₂ under HW for each year (red dots) plotted with the interannual variations of their annual-mean concentrations under nonHW (black solid line). The gray shaded area indicates one standard deviation of each pollutant under nonHW for each year.

Table 3

Correlation coefficients between daily concentrations of the six air pollutants ($\text{PM}_{2.5}$, PM_{10} , O_3 , NO_2 , CO , and SO_2) and the three meteorological variables (WS10_{avg} , $\text{WS850}_{\text{avg}}$, and BLH_{avg}) under HW. The numbers in the parentheses indicate those under nonHW.

	WS10_{avg}	$\text{WS850}_{\text{avg}}$	BLH_{avg}
$\text{PM}_{2.5}$	-0.38* (-0.20*)	-0.39* (-0.14*)	-0.47* (-0.27*)
PM_{10}	-0.29* (-0.19*)	-0.34* (-0.13*)	-0.42* (-0.32*)
O_3	-0.21* (-0.07*)	-0.33* (-0.21*)	0.07 (0.18*)
NO_2	-0.50* (-0.49*)	-0.40* (-0.37*)	-0.59* (-0.51*)
CO	-0.32* (-0.29*)	-0.34* (-0.28*)	-0.43* (-0.38*)
SO_2	-0.35* (-0.11*)	-0.08 (-0.16*)	-0.46* (-0.19*)

* Statistically significant ($p < 0.05$).

year, respectively. For $\text{PM}_{2.5}$, one HW day is excluded due to the missing values of $\text{PM}_{2.5}$ concentration. In the next two subsections, we examine how the varying air quality within HW is related to meteorological conditions and large-scale atmospheric patterns.

3.2. Varying air quality within HW and associated meteorological conditions

Table 3 shows correlation coefficients between daily concentrations of the six air pollutants ($\text{PM}_{2.5}$, PM_{10} , O_3 , NO_2 , CO , and SO_2) and the three meteorological variables (WS10_{avg} , $\text{WS850}_{\text{avg}}$, and BLH_{avg}) under HW and nonHW. The air pollutants have negative correlations with WS10_{avg} , $\text{WS850}_{\text{avg}}$, and BLH_{avg} under both HW and nonHW, except for the correlation between O_3 and BLH_{avg} . Among them, the correlation between NO_2 and BLH_{avg} under HW is the strongest ($R = -0.59$). Low WS10_{avg} , $\text{WS850}_{\text{avg}}$, and BLH_{avg} are favorable for the accumulation of air pollutants and therefore lead to their high concentrations. It is noticeable that the negative correlations become stronger under HW than under nonHW, except for the correlation between SO_2 and $\text{WS850}_{\text{avg}}$. In other words, the concentrations of the air pollutants under HW are more dependent on these meteorological variables than those under nonHW. Note that WS10_{avg} , $\text{WS850}_{\text{avg}}$, and BLH_{avg} are significantly correlated with each other, which may be explained by that high synoptic wind speed can increase near-surface wind speed and high near-surface wind speed can increase BLH (Hu et al., 2021).

To examine meteorological characteristics related to the varying air quality within HW, we divide HW into two periods for each pollutant. INC_x (DEC_x) is the HW days in which pollutant x shows increased (decreased) daily concentrations than its nonHW mean for the corresponding year, where x is $\text{PM}_{2.5}$, PM_{10} , O_3 , NO_2 , CO , or SO_2 . **Table 4** presents the mean daily concentration and the mean values of meteorological variables (T_{avg} , RH_{avg} , WS10_{avg} , $\text{WS850}_{\text{avg}}$, and BLH_{avg}) under INC_x and DEC_x for each pollutant. All the air pollutants show significant differences in concentrations between corresponding INC_x and DEC_x . The differences are largest for $\text{PM}_{2.5}$ and O_3 : their concentrations under INC_x are higher by 89 % and 71 %, respectively, than those under DEC_x . Interestingly, T_{avg} is not significantly different between INC_x and DEC_x for all the air pollutants except for O_3 . There are significant differences in WS10_{avg} , $\text{WS850}_{\text{avg}}$, and BLH_{avg} between INC_x and DEC_x , which can be expected from the strong negative correlations between the air pollutant concentrations and these variables under HW (**Table 3**). For all the air pollutants except for O_3 (SO_2), WS10_{avg} ($\text{WS850}_{\text{avg}}$) is significantly lower under INC_x than under DEC_x . BLH_{avg} is also significantly lower under INC_x for all the air pollutants except for O_3 . Consequently, the changes in WS10_{avg} , $\text{WS850}_{\text{avg}}$, and BLH_{avg} within HW largely contribute to the significant variability of air quality within HW and thus whether air quality worsens or not compared to nonHW.

3.3. Large-scale atmospheric patterns associated with varying air quality within HW

The significant differences in air quality and meteorological variables within HW could be associated with different large-scale atmospheric patterns. **Fig. 5** shows difference fields of 200- and 500-hPa geopotential heights between INC_x and DEC_x for the six air pollutants. At 200 hPa, a zonal wave-like pattern is seen (**Fig. 5a–e**) except for SO_2 . This zonal wave-like pattern is similar to the circumglobal teleconnection (CGT) pattern (Ding and Wang, 2005; Yeh et al., 2018; Choi et al., 2020). The CGT pattern is a recurrent zonal wave pattern in northern hemisphere summer maintained by the interactions between the Rossby wave train and the Indian summer monsoon (Ding and Wang, 2005; Ding et al., 2011). This CGT pattern is known as one of the major patterns that bring heat waves in South Korea (Yeh et al., 2018; Choi et al., 2020). Like in the CGT pattern identified by Yeh et al. (2018) and Choi et al. (2020), prominent positive

Table 4

Mean daily concentrations, T_{avg} , RH_{avg} , WS10_{avg} , $\text{WS850}_{\text{avg}}$, and BLH_{avg} under INC_x and DEC_x for each pollutant x ($\text{PM}_{2.5}$, PM_{10} , O_3 , NO_2 , CO , or SO_2) and their respective differences (INC_x minus DEC_x). For the differences, the statistical significances are given.

	Daily concentration	T_{avg} (°C)	RH_{avg} (%)	WS10_{avg} (m s^{-1})	$\text{WS850}_{\text{avg}}$ (m s^{-1})	BLH_{avg} (m)
$\text{PM}_{2.5}$ ($\mu\text{g m}^{-3}$)						
$\text{INC}_{\text{PM2.5}}$ [113 days]	26.6	29.6	63.4	1.44	4.58	428.4
$\text{DEC}_{\text{PM2.5}}$ [91 days]	14.0	29.5	63.3	1.71	6.03	507.6
$\text{INC}_{\text{PM2.5}} - \text{DEC}_{\text{PM2.5}}$	12.5*	0.2	0.1	-0.26*	-1.45*	-79.2*
PM_{10} ($\mu\text{g m}^{-3}$)						
INC_{PM10} [95 days]	45.0	29.6	63.5	1.41	4.41	418.5
DEC_{PM10} [110 days]	25.3	29.5	63.4	1.69	5.93	501.2
$\text{INC}_{\text{PM10}} - \text{DEC}_{\text{PM10}}$	19.8*	0.1	0.1	-0.27*	-1.52*	-82.6*
O_3 (ppb)						
INC_{O_3} [125 days]	34.5	29.8	61.6	1.51	4.52	463.0
DEC_{O_3} [80 days]	20.2	29.2	66.0	1.63	6.31	462.7
$\text{INC}_{\text{O}_3} - \text{DEC}_{\text{O}_3}$	14.3*	0.6*	-4.4*	-0.12	-1.79*	0.3
NO_2 (ppb)						
INC_{NO_2} [111 days]	26.0	29.5	63.5	1.38	4.55	417.5
DEC_{NO_2} [94 days]	17.7	29.6	63.3	1.77	6.01	516.5
$\text{INC}_{\text{NO}_2} - \text{DEC}_{\text{NO}_2}$	8.3*	-0.1	0.2	-0.39*	-1.46*	-99.0*
CO (ppb)						
INC_{CO} [92 days]	471.0	29.5	63.5	1.40	4.28	403.2
DEC_{CO} [113 days]	335.8	29.6	63.3	1.68	5.99	511.4
$\text{INC}_{\text{CO}} - \text{DEC}_{\text{CO}}$	135.2*	-0.1	0.2	-0.28*	-1.72*	-108.2*
SO_2 (ppb)						
INC_{SO_2} [102 days]	4.3	29.4	64.6	1.44	5.16	428.5
DEC_{SO_2} [103 days]	3.6	29.8	62.3	1.67	5.28	496.9
$\text{INC}_{\text{SO}_2} - \text{DEC}_{\text{SO}_2}$	0.8*	-0.4	2.3*	-0.23*	-0.12	-68.4*

* Statistically significant ($p < 0.05$).

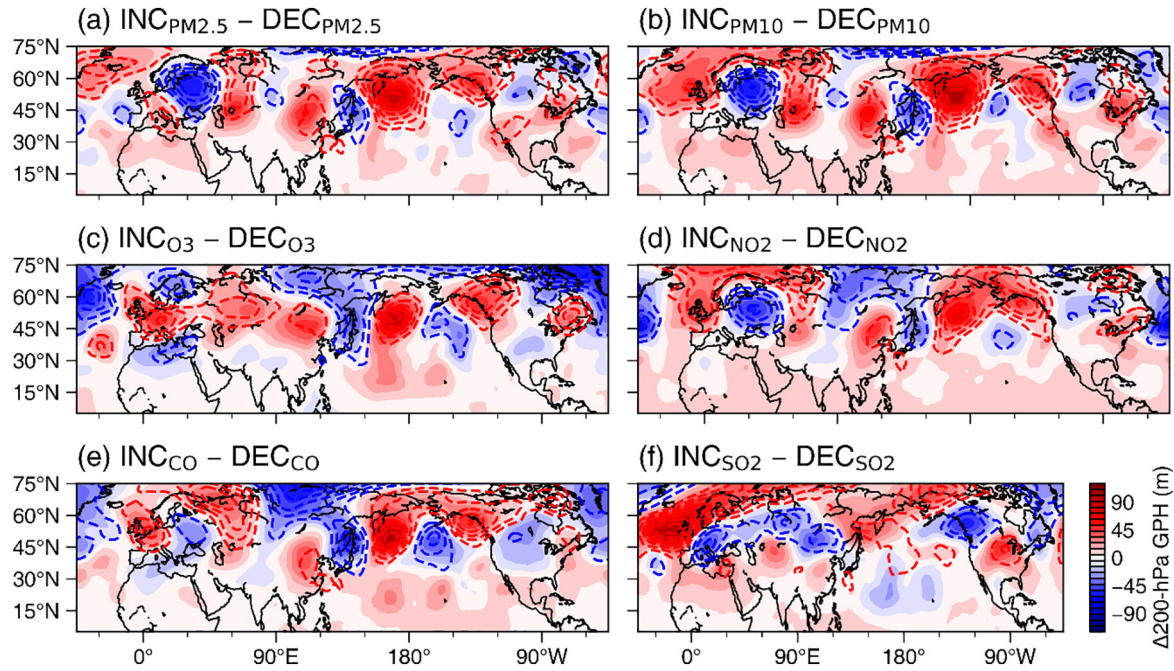


Fig. 5. Spatial distributions of differences in 200-hPa geopotential height (shaded) and 500-hPa geopotential height (contour) between INC_x and DEC_x for each pollutant x ($\text{PM}_{2.5}$, PM_{10} , O_3 , NO_2 , CO , or SO_2).

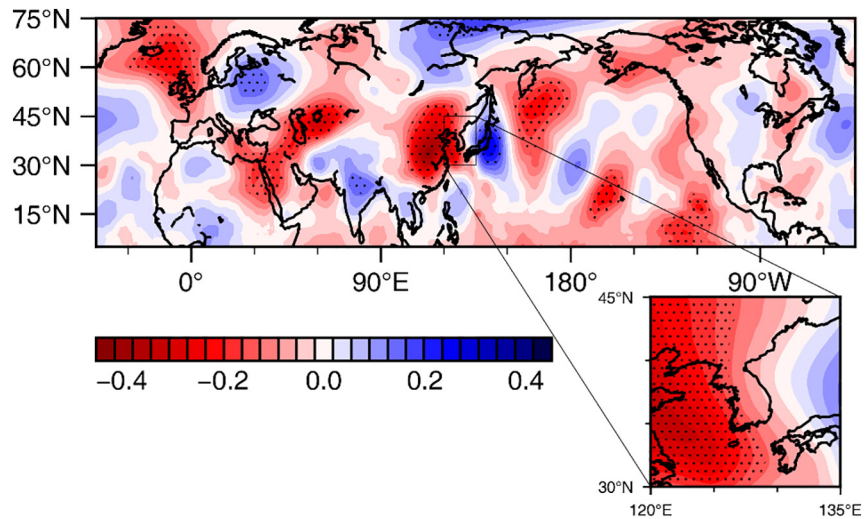
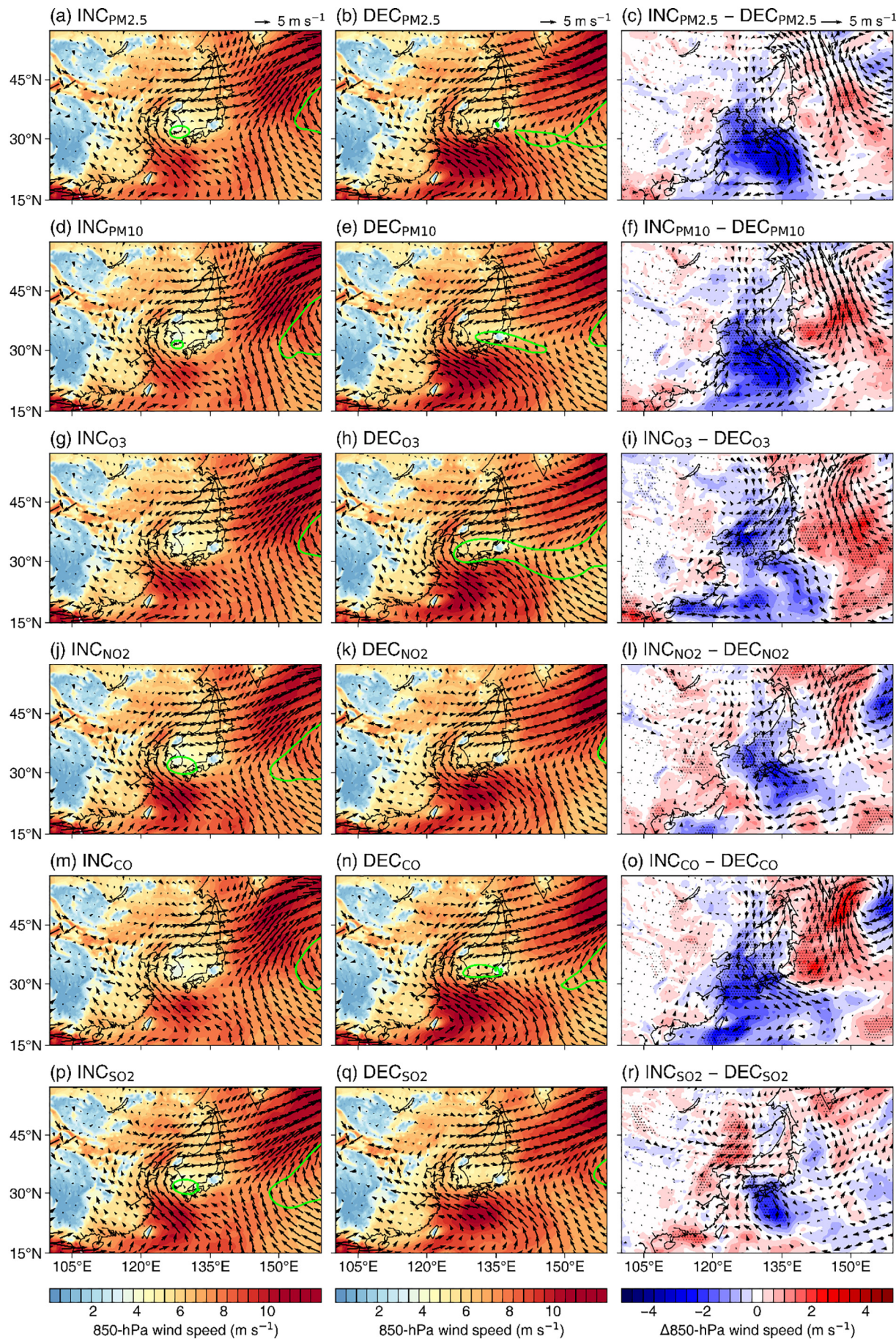


Fig. 6. Spatial distribution of the correlation coefficient between 850-hPa wind speed over the Korean Peninsula ($\text{WS850}_{\text{avg}}$) and 500-hPa geopotential height under HW. The dotted area indicates statistical significance at $p < 0.05$.

geopotential height differences (INC_x minus DEC_x) appear over Northwestern Europe, Central Asia, northeastern China ($\sim 30\text{--}45^\circ\text{N}$, $\sim 100\text{--}120^\circ\text{E}$), the Kamchatka Peninsula ($\sim 35\text{--}55^\circ\text{N}$, $\sim 150\text{--}175^\circ\text{E}$), and northwestern and northeastern parts of North America. The Korean Peninsula is located between the positive geopotential height difference over the northeastern China and the negative geopotential height difference over Japan ($\sim 30\text{--}45^\circ\text{N}$, $\sim 135\text{--}150^\circ\text{E}$). The geopotential height difference pattern at 500 hPa is very similar to that at 200 hPa, indicating the barotropic vertical structure of the wave-like pattern in the mid-to-upper troposphere.

How the wave-like pattern is related to the synoptic wind speed over the Korean Peninsula is examined. Fig. 6 presents the spatial distribution of correlation coefficient between 850-hPa wind speed over the Korean Peninsula ($\text{WS850}_{\text{avg}}$) and 500-hPa geopotential height at each grid point under HW. The correlation pattern is quite similar to the wave-like pattern seen in Fig. 5a–e, showing negative (positive) correlations over the regions of positive (negative) geopotential height differences in the wave-like pattern. $\text{WS850}_{\text{avg}}$ shows statistically significant correlations with the geopotential height over eastern China, Japan, and southeast of the Kamchatka

Fig. 7. Composite fields of 850-hPa horizontal wind speed (color shades) and wind vector (arrows) under (a, d, g, j, m, p) INC_x and (b, e, h, k, n, q) DEC_x and (c, f, i, l, o, r) their respective differences for each pollutant x ($\text{PM}_{2.5}$, PM_{10} , O_3 , NO_2 , CO , or SO_2). The green contour line indicates the 5880-m isoline. The dotted area in (c), (f), (i), (l), (o), and (r) indicates statistical significance at $p < 0.05$.



Peninsula. The statistical significance also appears over Northwestern Europe and Central Asia which are upstream regions of the wave-like pattern with the positive geopotential height differences (Fig. 5a–e). Thus, the wave-like pattern under HW has significant associations with the synoptic wind speed over the Korean Peninsula.

Under DEC_x except for DEC_{SO2}, the center of high pressure is located to the northeast of the Korean Peninsula (not shown). The center becomes close to the Korean Peninsula under INC_x except for INC_{SO2}, associated with the positive geopotential height difference over northeastern China and the negative geopotential height difference over Japan (Fig. 5a–e). This leads to stronger vertical subsidence at the mid-to-upper troposphere and lower WS850_{avg}. The positive difference over the Kamchatka Peninsula (Fig. 5a–e) may act as a blocking high, causing stagnant conditions over the Korean Peninsula. The blocking high over the Kamchatka Peninsula obstructs the eastward movement of upstream weather systems and thus brings persistent and stagnant weather conditions over the Korean Peninsula, which may cause heat waves and worsen air quality (Yeh et al., 2018; Yun and Yoo, 2019; Ku et al., 2021).

Relationships between the large-scale atmospheric patterns around the Korean Peninsula and WS850_{avg} are further examined. Fig. 7 shows composite fields of 850-hPa horizontal wind speed and wind vector under INC_x and DEC_x and their respective differences for the six air pollutants. Under both INC_x and DEC_x, anticyclonic circulation is dominant over South Korea. Due to the negative geopotential height difference over Japan under INC_x except for INC_{SO2}, the wind differences over South Korea are northerly/northeasterly (Fig. 7c, f, i, l, and o). These wind differences counteract the prevailing anticyclonic circulation and thus reduce WS850_{avg}. To the south of the Kamchatka Peninsula, the westerly winds slant to the meridional direction as the blocking high over the southeast of the Kamchatka Peninsula obstructs zonal flows. When a cyclonic circulation over Japan in the difference field is evident associated with the negative geopotential height difference there (Fig. 7c, f, i, and o), the expansion of the WNPSH is inhibited. This also contributes to the significant correlation between WS850_{avg} and the negative geopotential height difference over Japan (Fig. 6) since relatively high wind speed appears along the southwestern boundary of the WNPSH.

The results from Table 4 and Figs. 5–7 suggest that heat waves occurring with the wave-like pattern bring more stagnant conditions over Seoul and therefore significantly higher PM_{2.5}, PM₁₀, O₃, NO₂, and CO concentrations than heat waves without this pattern. SO₂ seems to be less influenced by the synoptic winds and large-scale atmospheric patterns than other air pollutants.

3.4. Other meteorological factors contributing to the O₃ variability within HW

Unlike the other pollutants, the O₃ concentration under HW significantly varies with temperature as well as with wind speed (Table 4). To examine the relationship between O₃ concentration and temperature, scatterplots of the daily maximum of 8-hour average O₃ concentration (MDA8) versus T_{max} and daily total insolation are shown in Fig. 8. MDA8 and T_{max} have a significant positive correlation with the correlation coefficient of 0.40 under HW. The slope of the linear regression of MDA8 on T_{max} is 6.24 ppb °C⁻¹. However, the correlation between MDA8 and T_{max} is relatively small compared to the relationships between O₃ concentration and temperature that were reported in other cities (e.g., Rasmussen et al., 2012; Gu et al., 2020). As revealed in Tables 3 and 4, this comes from that in Seoul, wind speed is also crucial for determining O₃ concentration besides temperature. Interestingly, the correlation between MDA8 and daily total insolation under HW is insignificant (Fig. 8b). It may indicate that under high-insolation conditions brought by heat waves, an increase in insolation does not necessarily lead to an increase in O₃ concentration and the direct effects of temperature on O₃ production become more important. High temperature directly increases O₃ concentration by increasing chemical reaction rates and emissions of biogenic volatile organic compounds (VOCs) such as isoprene (Coates et al., 2016). Especially, a number of studies revealed that enhanced biogenic VOCs emissions during heat waves considerably increase O₃ concentration in urban areas (e.g., Solberg et al., 2008; Churkina et al., 2017; Ma et al., 2019; Wang et al., 2021).

To compare the relative importance of temperature to the O₃ concentration under HW with those of other meteorological variables, the multiple linear regression analysis is conducted. T_{max}, daytime relative humidity, daytime 10-m wind speed, daytime BLH, daily total insolation, and WS850_{avg} are used as predictors, and all variables are standardized. The multiple linear regression explains 44.4 % of the total variance of MDA8 within HW. The regression coefficients are -0.30 for daytime 10-m wind speed, -0.25 for WS850_{avg}, 0.23 for T_{max}, -0.21 for relative humidity, -0.09 for BLH, and 0.00 for daily total insolation, where those of BLH and daily total insolation are not statistically significant. This indicates that the relative importances of near-surface wind speed, synoptic wind speed, and relative humidity are comparable to that of near-surface temperature.

4. Summary and conclusions

This study examines changes in PM_{2.5}, PM₁₀, O₃, NO₂, CO, and SO₂ concentrations in Seoul during heat waves. For this, air quality data from 25 AQMSs and meteorological data from 23 surface weather stations and the

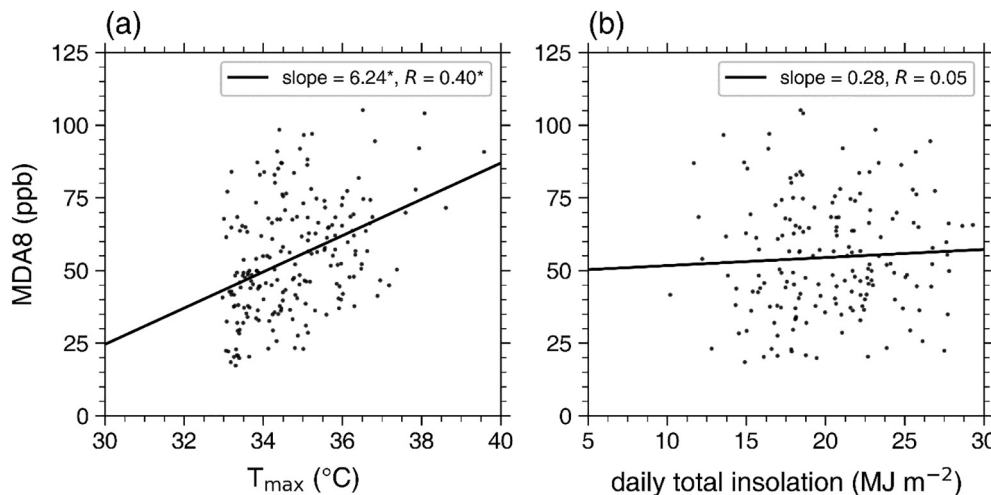


Fig. 8. Scatterplots of MDA8 versus (a) T_{max} and (b) daily total insolation under HW. The solid line indicates linear regression line. The asterisk (*) denotes the statistical significance at $p < 0.05$.

ERA5 during July and August of 2001–2021 are used. Under HW, the mean daily PM₁₀, NO₂, and CO concentrations decrease by 7.9 %, 6.1 %, and 4.6 %, respectively, and the mean daily PM_{2.5}, O₃, and SO₂ concentrations increase by 4.1 %, 17.2 %, and 2.9 %, respectively. The atmospheric circulation under heat waves is less favorable for long-range transport of air pollutants to Seoul. The prominent increase in O₃ concentration is caused by high temperature and high insolation during the daytime under HW. 37 % of the HW days exceed the O₃ concentration standard in South Korea. The increase in PM_{2.5} concentration can be due to enhanced secondary formation of aerosols under the high O₃ concentration. The decreases in NO₂ and CO concentrations can be due to relatively high BLH during the daytime and active chemical reactions and consumption of NO₂ and CO associated with the high O₃ concentration under HW. The slight increase in SO₂ concentration is possibly related to the increased emissions which result from increased cooling demands under HW.

Air quality in Seoul significantly depends on WS10_{avg}, WS850_{avg}, and BLH_{avg}, and this dependence becomes more prominent under HW. When the PM_{2.5}, PM₁₀, O₃, NO₂, and CO concentrations under HW are higher than those under nonHW, a zonal wave-like pattern of geopotential height differences similar to the CGT pattern is pronounced. This wave-like pattern is significantly associated with the decrease in synoptic wind speed and brings stagnant conditions over the Korean Peninsula. The O₃ concentration under HW is significantly correlated with temperature as well as with wind speed. However, daily total insolation does not have a significant correlation with O₃ concentration under HW. These imply the importance of the direct effects of temperature on O₃ production such as increasing chemical reaction rates and increasing emissions of precursors such as biogenic VOCs under heat waves.

This study reveals that there is a significant variability of air quality within heat waves, and it is associated with large-scale atmospheric patterns. The transport of air pollutants and precursors by local winds such as urban breezes, land/sea breezes, and mountain/valley winds is also an important factor affecting the air quality in Seoul (Ryu et al., 2013; Lee et al., 2014). How the local winds change under heat waves and how this change affects air quality deserve future investigation using a coupled meteorology-air quality model. Given the relationship between O₃ concentration and temperature in Seoul, the urban heat islands in Seoul and their interactions with heat waves are expected to have some effects on O₃ concentration. Quantifying these effects will give further insights into O₃ air quality in urban areas.

Changes in human activities during heat waves can also have an impact on air quality. For instance, increased cooling demand during heat waves may enhance the emission of air pollutants from power plants (Abel et al., 2017). Future investigation on the contribution of human activity changes to the air quality changes under heat waves will help to better understand the impacts of heat waves on air quality.

CRediT authorship contribution statement

Kyeongjoo Park: Methodology, Validation, Formal analysis, Investigation, Data curation, Writing – original draft, Writing – review & editing, Visualization. **Han-Gyul Jin:** Conceptualization, Formal analysis, Supervision, Writing – review & editing. **Jong-Jin Baik:** Conceptualization, Methodology, Supervision, Writing – review & editing.

Data availability

Data will be made available on request.

Declaration of competing interest

The authors declare that they have no known competing financial interests or personal relationships that could have appeared to influence the work reported in this paper.

Acknowledgements

The authors are grateful to two anonymous reviewers for providing valuable comments on this work. This work was supported by the National Research Foundation of Korea (2021R1A2C1007044).

References

- Abel, D., Holloway, T., Kladar, R.M., Meier, P., Ahl, D., Harkey, M., Patz, J., 2017. Response of power plant emissions to ambient temperature in the eastern United States. *Environ. Sci. Technol.* **51**, 5838–5846.
- Allabakash, S., Lim, S., 2020. Climatology of planetary boundary layer height-controlling meteorological parameters over the Korean Peninsula. *Remote Sens.* **12**, 2571.
- Amengual, A., Homar, V., Romero, R., Brooks, H.E., Ramis, C., Gordaliza, M., Alonso, S., 2014. Projections of heat waves with high impact on human health in Europe. *Glob. Planet. Change* **119**, 71–84.
- Bae, C., Kim, B.-U., Kim, H.C., Yoo, C., Kim, S., 2020. Long-range transport influence on key chemical components of PM_{2.5} in the Seoul metropolitan area, South Korea, during the years 2012–2016. *Atmosphere* **11**, 48.
- Barriopedro, D., Fischer, E.M., Luterbacher, J., Trigo, R.M., García-Herrera, R., 2011. The hot summer of 2010: redrawing the temperature record map of Europe. *Science* **332**, 220–224.
- BCCS, 2022. Extreme Heat And Human Mortality: A Review of Heat-related Deaths in B.C. in Summer 2021. British Columbia Coroners Services, British Columbia.
- Cha, Y., Choi, J., Kim, E.-S., Ahn, J.-B., 2022. Occurrence of heatwave in Korea by the displacement of South Asian high. *Clim. Dyn.* **58**, 1699–1718.
- Chen, S., Huang, J., Kang, L., Wang, H., Ma, X., He, Y., Yuan, T., Yang, B., Huang, Z., Zhang, G., 2017. Emission, transport, and radiative effects of mineral dust from the Taklimakan and Gobi deserts: comparison of measurements and model results. *Atmos. Chem. Phys.* **17**, 2401–2421.
- Chen, S., Wang, H., Lu, K., Zeng, L., Hu, M., Zhang, Y., 2020. The trend of surface ozone in Beijing from 2013 to 2019: indications of the persisting strong atmospheric oxidation capacity. *Atmos. Environ.* **242**, 117801.
- Choi, N., Lee, M.-I., Cha, D.-H., Lim, Y.-K., Kim, K.-M., 2020. Decadal changes in the interannual variability of heat waves in East Asia caused by atmospheric teleconnection changes. *J. Clim.* **33**, 1505–1522.
- Choi, W., Ho, C.-H., Jung, J., Chang, M., Ha, K.-J., 2021. Synoptic conditions controlling the seasonal onset and days of heatwaves over Korea. *Clim. Dyn.* **57**, 3045–3053.
- Churkina, G., Kuik, F., Bonn, B., Lauer, A., Grote, R., Tomiak, K., Butler, T.M., 2017. Effect of VOC emissions from vegetation on air quality in Berlin during a heatwave. *Environ. Sci. Technol.* **51**, 6120–6130.
- Coates, J., Mar, K.A., Ojha, N., Butler, T.M., 2016. The influence of temperature on ozone production under varying NO_x conditions – a modelling study. *Atmos. Chem. Phys.* **16**, 11601–11615.
- Ding, Q., Wang, B., 2005. Circumglobal teleconnection in the Northern Hemisphere summer. *J. Clim.* **18**, 3483–3505.
- Ding, Q., Wang, B., Wallace, J.M., Branstator, G., 2011. Tropical-extratropical teleconnections in boreal summer: observed interannual variability. *J. Clim.* **24**, 1878–1896.
- Fischer, P.H., Brunekreef, B., Lebret, E., 2004. Air pollution related deaths during the 2003 heat wave in the Netherlands. *Atmos. Environ.* **38**, 1083–1085.
- Gelaro, R., McCarty, W., Suárez, M.J., Todling, R., Molod, A., Takacs, L., Randles, C.A., Darmenov, A., Bosilovich, M.G., Reichle, R., Wargan, K., Coy, L., Cullather, R., Draper, C., Akella, S., Buchard, V., Conaty, A., da Silva, A.M., Gu, W., Kim, G.-K., Koster, R., Lucchesi, R., Merkova, D., Nielsen, J.E., Partyka, G., Pawson, S., Putman, W., Riendecker, M., Schubert, S.D., Sienkiewicz, M., Zhao, B., 2017. The modern-era retrospective analysis for research and applications, version 2 (MERRA-2). *J. Clim.* **30**, 5419–5454.
- Ghim, Y.S., Chang, Y.-S., Jung, K., 2015. Temporal and spatial variations in fine and coarse particles in Seoul, Korea. *Aerosol Air Qual. Res.* **15**, 842–852.
- Goklany, I.M., 2009. Deaths and death rates from extreme weather events: 1900–2008. *J. Am. Phys. Surg.* **14**, 102–109.
- Gu, Y., Li, K., Xu, J., Liao, H., Zhou, G., 2020. Observed dependence of surface ozone on increasing temperature in Shanghai, China. *Atmos. Environ.* **221**, 117108.
- Guo, J., Zhang, J., Yang, K., Liao, H., Zhang, S., Huang, K., Lv, Y., Shao, J., Yu, T., Tong, B., Li, J., Su, T., Yin, S.H.L., Stoffelen, A., Zhai, P., Xu, X., 2021. Investigation of near-global daytime boundary layer height using high-resolution radiosondes: first results and comparison with ERA5, MERRA-2, JRA-55, and NCEP-2 reanalyses. *Atmos. Chem. Phys.* **21**, 17079–17097.
- Hersbach, H., Bell, B., Berrisford, P., Hirahara, S., Horányi, A., Muñoz-Sabater, J., Nicolas, J., Peubey, C., Radu, R., Schepers, D., Simmons, A., Soci, C., Abdalla, S., Abellán, X., Balsamo, G., Bechtold, P., Biavati, G., Bidlot, J., Bonavita, M., Chiara, G.D., Dahlgren, P., Dee, D., Diamantakis, M., Dragani, R., Flemming, J., Forbes, R., Fuentes, M., Geer, A., Haimberger, L., Healy, S., Hogan, R.J., Hólm, E., Janisková, M., Keeley, S., Laloyaux, P., Lopez, P., Lupu, C., Radnoti, G., de Rosnay, P., Rozum, I., Vamborg, F., Villaume, S., Thépaut, J.-N., 2020. The ERA5 global reanalysis. *Q. J. R. Meteorol. Soc.* **146**, 1999–2049.
- Hong, J.-W., Hong, J., Kwon, E.E., Yoon, D.K., 2019. Temporal dynamics of urban heat island correlated with the socio-economic development over the past half-century in Seoul, Korea. *Environ. Pollut.* **254**, 112934.
- Huo, Y., Wang, Y., Paasonen, P., Liu, Q., Tang, G., Ma, Y., Petaja, T., Kerminen, V.-M., Kulmala, M., 2021. Trends of planetary boundary layer height over urban cities of China from 1980–2018. *Front. Environ. Sci.* **9**, 744255.
- Inness, A., Ades, M., Agustí-Panareda, A., Barré, J., Benedictow, A., Blechschmidt, A.-M., Dominguez, J.J., Engelen, R., Eskes, H., Flemming, J., Huijnen, V., Jones, L., Kipling, Z., Massart, S., Parrington, M., Peuch, V.-H., Razinger, M., Remy, S., Schulz, M., Suttie,

- M., 2019. The CAMS reanalysis of atmospheric composition. *Atmos. Chem. Phys.* 19, 3515–3556.
- Jeong, U., Kim, J., Lee, H., Lee, Y.G., 2017. Assessing the effect of long-range pollutant transportation on air quality in Seoul using the conditional potential source contribution function method. *Atmos. Environ.* 150, 33–44.
- Jin, C., Wang, Y., Li, T., Yuan, Q., 2022. Global validation and hybrid calibration of CAMS and MERRA-2 PM_{2.5} reanalysis products based on OpenAQ platform. *Atmos. Environ.* 274, 118972.
- Kalisa, E., Fadlallah, S., Amani, M., Nahayo, L., Habiyaremye, G., 2018. Temperature and air pollution relationship during heatwaves in Birmingham, UK. *Sustain. Cities Soc.* 43, 111–120.
- Kim, D., Choi, H.-E., Gal, W.-M., Seo, S., 2020. Five year trends of particulate matter concentrations in Korean regions (2015–2019): when to ventilate? *Int. J. Environ. Res. Public Health* 17, 5764.
- Kim, D.-W., Deo, R.C., Chung, J.-H., Lee, J.-S., 2016. Projection of heat wave mortality related to climate change in Korea. *Nat. Hazards* 80, 623–637.
- Kim, K.-Y., 2022. Diurnal and seasonal variation of planetary boundary layer height over East Asia and its climatic change as seen in the ERA-5 reanalysis data. *SN Appl. Sci.* 4, 39.
- Kim, N.K., Kim, I.S., Song, I.H., Park, S.M., Lim, H.B., Kim, Y.P., Shin, H.J., Lee, J.Y., 2021. Temporal variation of sulfate concentration in PM_{2.5} and major factors enhancing sulfate concentration in the atmosphere of Seoul, Korea. *Air Qual. Atmos. Health* 14, 985–999.
- Kim, S., Jeong, D., Sanchez, D., Wang, M., Seco, R., Blake, D., Meinardi, S., Barletta, B., Hughes, S., Jung, J., Kim, D., Lee, G., Lee, M., Ahn, J., Lee, S.-D., Cho, G., Sung, M.-Y., Lee, Y.-H., Park, R., 2018. The controlling factors of photochemical ozone production in Seoul, South Korea. *Aerosol Air Qual. Res.* 18, 2253–2261.
- Kim, S.-U., Kim, K.-Y., 2020. Physical and chemical mechanisms of the daily-to-seasonal variation of PM₁₀ in Korea. *Sci. Total Environ.* 712, 136429.
- Kim, Y.P., Lee, G., 2018. Trend of air quality in Seoul: policy and science. *Aerosol Air Qual. Res.* 18, 2141–2156.
- Ku, H.-Y., Noh, N., Jeong, J.-H., Koo, J.-H., Choi, W., Kim, B.-M., Lee, D., Ban, S.-J., 2021. Classification of large-scale circulation patterns and their spatio-temporal variability during High-PM₁₀ events over the Korean Peninsula. *Atmos. Environ.* 262, 118632.
- Lee, W.-S., Lee, M.-I., 2016. Interannual variability of heat waves in South Korea and their connection with large-scale atmospheric circulation patterns. *Int. J. Climatol.* 36, 4815–4830.
- Lee, H.-M., Park, R.J., 2022. Factors determining the seasonal variation of ozone air quality in South Korea: regional background versus domestic emission contributions. *Environ. Pollut.* 308, 119645.
- Lee, K.-Y., Kwak, K.-H., Ryu, Y.-H., Lee, S.-H., Baik, J.-J., 2014. Impacts of biogenic isoprene emission on ozone air quality in the Seoul metropolitan area. *Atmos. Environ.* 96, 209–219.
- Lee, G., Oh, H.-R., Ho, C.-H., Park, D.-S.R., Kim, J., Chang, L.-S., Lee, J.-B., Choi, J., Sung, M., 2018. Slow decreasing tendency of fine particles compared to coarse particles associated with recent hot summers in Seoul, Korea. *Aerosol Air Qual. Res.* 18, 2185–2194.
- Lee, H.-D., Min, K.-H., Bae, J.-H., Cha, D.-H., 2020a. Characteristics and comparison of 2016 and 2018 heat wave in Korea. *Atmosphere* 30, 1–15 (in Korean with English abstract).
- Lee, H.K., Choi, E.L., Lee, H.J., Lee, S.Y., Lee, J.Y., 2020b. A study on the seasonal correlation between O₃ and PM_{2.5} in Seoul in 2017. *J. Korean Soc. Atmos. Environ.* 36, 533–542 (in Korean with English abstract).
- Lee, S., Kim, M., Kim, S.-Y., Lee, D.-W., Lee, H., Kim, J., Le, S., Liu, Y., 2021. Assessment of long-range tranboundary aerosols in Seoul, South Korea from Geostationary Ocean Color Imager (GOCCI) and ground-based observations. *Environ. Pollut.* 269, 115924.
- Li, Z., Wang, Y., Guo, J., Zhao, C., Cribb, M.C., Dong, X., Fan, J., Gong, D., Huang, J., Jiang, M., Jiang, Y., Lee, S.-S., Li, H., Li, J., Liu, J., Qian, Y., Rosenfeld, D., Shan, S., Sun, Y., Wang, H., Xin, J., Yan, X., Yang, X., Yang, X.-q., Zhang, F., Zheng, Y., 2019. East Asian study of tropospheric aerosols and their impact on regional clouds, precipitation, and climate (EAST-AIR_{CPC}), 2019. *J. Geophys. Res. Atmos.* 124, 13026–13054.
- Ma, M., Gao, Y., Wang, Y., Zhang, S., Leung, L.R., Liu, C., Wang, S., Zhao, B., Chang, X., Su, H., Zhang, T., Sheng, L., Yao, X., Gao, H., 2019. Substantial ozone enhancement over the North China Plain from increased biogenic emissions due to heat waves and land cover in summer 2017. *Atmos. Chem. Phys.* 19, 12195–12207.
- Martilli, A., 2002. Numerical study of urban impact on boundary layer structure: sensitivity to wind speed, urban morphology, and rural soil moisture. *J. Appl. Meteorol. Climatol.* 41, 1247–1266.
- Noh, E., Kim, J., Jun, S.-Y., Cha, D.-H., Park, M.-S., Kim, J.-H., Kim, H.-G., 2021. The role of the Pacific-Japan pattern in extreme heatwaves over Korea and Japan. *Geophys. Res. Lett.* 48, e2021GL093990.
- Papanastasiou, D.K., Melas, D., Bartzanas, T., Kittas, C., 2010. Temperature, comfort and pollution levels during heat waves and the role of sea breeze. *Int. J. Biometeorol.* 54, 307–317.
- Papanastasiou, D.K., Melas, D., Kambezidis, H.D., 2015. Air quality and thermal comfort levels under extreme hot weather. *Atmos. Res.* 152, 4–13.
- Park, D.-H., Kim, S.-W., Kim, M.-H., Yeo, H., Park, S.S., Nishizawa, T., Shimizu, A., Kim, C.-H., 2021. Impacts of local versus long-range transported aerosols on PM₁₀ concentrations in Seoul, Korea: an estimate based on 11-year PM₁₀ and lidar observations. *Sci. Total Environ.* 750, 141739.
- Park, J., Chae, Y., 2020. Analysis of heat-related illness and excess mortality by heat waves in South Korea in 2018. *J. Korean Geogr. Soc.* 55, 391–408 (in Korean with English abstract).
- Park, J., Kim, H., Kim, Y., Heo, J., Kim, S.-W., Jeon, K., Yi, S.-M., Hopke, P.K., 2022. Source apportionment of PM_{2.5} in Seoul, South Korea and Beijing, China using dispersion normalized PMF. *Sci. Total Environ.* 833, 155056.
- Park, S., Son, S.-W., Jung, M.-I., Park, J., Park, S.S., 2020. Evaluation of tropospheric ozone reanalyses with independent ozonesonde observations in East Asia. *Geosci. Lett.* 7, 12.
- Peng, R.D., Bobb, J.F., Tebaldi, C., McDaniel, L., Bell, M.L., Dominici, F., 2011. Toward a quantitative estimate of future heat wave mortality under global climate change. *Environ. Health Perspect.* 119, 701–706.
- Pu, X., Wang, T.J., Huang, X., Melas, D., Zanis, P., Papanastasiou, D.K., Poupkou, A., 2017. Enhanced surface ozone during the heat wave of 2013 in Yangtze River Delta region, China. *Sci. Total Environ.* 603–604, 807–816.
- Pyrigou, A., Hadjinicolaou, P., Santamouris, M., 2018. Enhanced near-surface ozone under heatwave conditions in a Mediterranean island. *Sci. Rep.* 8, 9191.
- Rasmussen, D.J., Fiore, A.M., Naik, V., Horowitz, L.W., McGinnis, S.J., Schultz, M.G., 2012. Surface ozone-temperature relationships in the eastern US: a monthly climatology for evaluating chemistry-climate models. *Atmos. Environ.* 47, 142–153.
- Robine, J.-M., Cheung, S.L.K., Le Roy, S., Van Oyen, H., Griffiths, C., Michel, J.-P., Herrmann, F.R., 2008. Death toll exceeded 70,000 in Europe during the summer of 2003. *C. R. Biol.* 331, 171–178.
- Ruiz-Páez, R., Díaz, J., López-Bueno, J.A., Navas, M.A., Mirón, I.J., Martínez, G.S., Luna, M.Y., Linares, C., 2023. Does the meteorological origin of heat waves influence their impact on health? A 6-year morbidity and mortality study in Madrid (Spain). *Sci. Total Environ.* 855, 158900.
- Ryu, Y.-H., Baik, J.-J., Kwak, K.-H., Kim, S., Moon, N., 2013. Impacts of urban land-surface forcing on ozone air quality in the Seoul metropolitan area. *Atmos. Chem. Phys.* 13, 2177–2194.
- Seo, J., Park, D.-S.R., Kim, J.Y., Youn, D., Lim, Y.B., Kim, Y., 2018. Effects of meteorology and emissions on urban air quality: a quantitative statistical approach to long-term records (1999–2016) in Seoul, South Korea. *Atmos. Chem. Phys.* 18, 16121–16137.
- Slättberg, N., Lai, H.-W., Chen, X., Ma, Y., Chen, D., 2022. Spatial and temporal patterns of planetary boundary layer height during 1979–2018 over the Tibetan Plateau using ERA5. *Int. J. Climatol.* 42, 3360–3377.
- Solberg, S., Hov, Ø., Søvde, A., Isaksen, I.S.A., Coddeville, P., De Backer, H., Forster, C., Orsolini, Y., Uhse, K., 2008. European surface ozone in the extreme summer 2003. *J. Geophys. Res. Atmos.* 113, D07307.
- Stedman, J.R., 2004. The predicted number of air pollution related deaths in the UK during the August 2003 heatwave. *Atmos. Environ.* 38, 1087–1090.
- Theoharatos, G., Pantavou, K., Mavrakis, A., Spanou, A., Katavoutas, G., Efstatithou, P., Mpekas, P., Asimakopoulos, D., 2010. Heat waves observed in 2007 in Athens, Greece: synoptic conditions, bioclimatological assessment, air quality levels and health effects. *Environ. Res.* 110, 152–161.
- Tong, N.Y.O., Leung, D.Y.C., Liu, C.-H., 2011. A review on ozone evolution and its relationship with boundary layer characteristics in urban environments. *Water Air Soil Pollut.* 214, 13–36.
- Tressol, M., Ordóñez, C., Zbinden, R., Brioude, J., Thouret, V., Mari, C., Nedelec, P., Cammas, J.-P., Smit, H., Patz, H.-W., Volz-Thomas, A., 2008. Air pollution during the 2003 European heat wave as seen by MOZAIC airliners. *Atmos. Chem. Phys.* 8, 2133–2150.
- Wang, H., Wu, K., Liu, Y., Sheng, B., Lu, X., He, Y., Xie, J., Wang, H., Fan, S., 2021. Role of heat wave-induced biogenic VOC enhancements in persistent ozone episodes formation in Pearl River Delta. *J. Geophys. Res. Atmos.* 126, e2020JD034317.
- Wang, L., Zhao, B., Zhang, Y., Hu, H., 2023. Correlation between surface PM_{2.5} and O₃ in eastern China during 2015–2019: spatiotemporal variations and meteorological impacts. *Atmos. Environ.* 294, 119520.
- Wang, Z., Li, Y., Chen, T., Zhang, D., Sun, F., Wei, Q., Dong, X., Sun, R., Huan, N., Pan, L., 2015. Ground-level ozone in urban Beijing over a 1-year period: temporal variations and relationship to atmospheric oxidation. *Atmos. Res.* 164–165, 110–117.
- Wu, J.-B., Wang, Q., Chen, H., Zhang, Y., Wild, O., 2017. On the origin of surface ozone episode in Shanghai over Yangtze River Delta during a prolonged heat wave. *Aerosol Air Qual. Res.* 17, 2804–2815.
- Wu, Y., Zhao, K., Huang, J., Arend, M., Gross, B., Moshary, F., 2019. Observation of heat wave effects on the urban air quality and PBL in New York City area. *Atmos. Environ.* 218, 117024.
- Yang, X., Zeng, G., Iyakaremye, V., Zhu, B., 2022. Effects of different types of heat wave days on ozone pollution over Beijing-Tianjin-Hebei and its future projection. *Sci. Total Environ.* 837, 155762.
- Yeh, S.-W., Won, Y.-J., Hong, J.-S., Lee, K.-J., Kwon, M., Seo, K.-H., Ham, Y.-G., 2018. The record-breaking heat wave in 2016 over South Korea and its physical mechanism. *Mon. Weather Rev.* 146, 1463–1474.
- Yeo, S.-R., Yeh, S.-W., Lee, W.-S., 2019. Two types of heat wave in Korea associated with atmospheric circulation pattern. *J. Geophys. Res. Atmos.* 124, 7498–7511.
- Yoon, D., Cha, D.-H., Lee, M.-I., Min, K.-H., Kim, J., Jun, S.-Y., Choi, Y., 2020. Recent changes in heatwave characteristics over Korea. *Clim. Dyn.* 55, 1685–1696.
- Yun, S.-G., Yoo, C., 2019. The effects of spring and winter blocking on PM₁₀ concentration in Korea. *Atmosphere* 10, 410.
- Zhang, Y.-L., Cao, F., 2015. Fine particulate matter (PM_{2.5}) in China at a city level. *Sci. Rep.* 5, 14884.
- Zhao, K., Bao, Y., Huang, J., Wu, Y., Moshary, F., Arend, M., Wang, Y., Lee, X., 2019. A high-resolution modeling study of a heat wave-driven ozone exceedance event in New York City and surrounding regions. *Atmos. Environ.* 199, 368–379.